Ti$_x$O$_y$ thin films with extremely low extinction coefficients obtained by pulsed magnetron sputtering

V. JOKANOVIĆ[a,b*], B. ČOLOVIĆ[a], N. BUNDALESKI[a], M. JOKANOVIĆ[b], A. TRAJKOVSKA PETKOSKA[c],
M. FERRARA[d], I. NASOV[e], Z. RAKOČEVIĆ[a]

[a]Vinča Institute of Nuclear Sciences, University of Belgrade, Mike Petrovića Alasa 12 -14, 11001 Belgrade, Serbia
[b]ALBOS d.o.o., Orahovačka 19, 11000 Belgrade, Serbia
[c]University St. Kliment Ohridski, Faculty of Technology and Technical Sciences, Titogradska 42, 1400 Veles, R. Macedonia
[d]DTE-STT-SCIS, Laboratorio sviluppo componenti ed impianti solari, Piazzale Enrico Fermi 1, 80055 Portici (NA), Italia
[e]Plasma d.o.o., 29 November 66/9, 1000 Skopje, R. Macedonia

Optical properties of Ti$_x$O$_y$ thin film, of thickness 125 nm, obtained by pulsed magnetron sputtering were investigated in this paper. XRD analysis revealed the presence of anatase, rutile, TiO, Ti$_2$O$_3$ and Ti$_3$O$_5$ phases. XPS analysis showed similar results. SEM analysis showed quite smooth surface of the film. Spectroscopic ellipsometry revealed sharp decrease of refractive index in wavelength range 300-500 nm and extremely low values of extinction coefficients which are less than 0.01 at wavelengths equal to or higher than 500 nm.

1. Introduction

Pulsed magnetron sputtering (PMS) offers stable deposition of defect free dielectric films because it prevents arcing at the target surface, thus allowing trouble free deposition [1]. Among numerous operational parameters, the most important ones are pulse frequency, reverse time, duty and reverse voltage, which can provide arc free operating conditions for a specific type of material, long-term process stability, important for improved coating properties, enhanced deposition rates, and reduced number of film defects [2]. Pulsed magnetron sputtering has been widely used in many commercial high-rate deposition processes for the production of solar cells and barrier coatings for food packaging [3].

It is well known that the microstructure and the phase composition of a film during magnetron sputtering depend mainly on the energy transferred from the plasma to the growing film, which can be successfully controlled by varying the flux and/or the energy of the bombarding ion species [4, 5]. Otherwise, in PMS, the ratio of ions to neutrals that bombard a growing film, most frequently is varied by changing the orientation of the substrate towards the ion beam source. Besides, the flux of negative oxygen ions can also be varied by changing the deposition angle [6, 7]. A number of studies have shown that the energetic bombardment during PMS not only influences the film densification and its surface smoothening, but also allows tailoring of the phase composition of the deposited film [8, 9].

PMS processes enable good film adhesion and large-scale uniformity of the film thickness distribution [10]. Moreover, sputtering is suitable for low temperature film growth because the sputtered ions have high enough energy for the enhancement of the crystallization rate. Furthermore, pulsed sputtering enables higher plasma density and higher energy of charged particles compared to the DC sputtering method [11, 12].

The correct selection of pulse parameters (frequency, duty cycle, reverse voltage) ensures extended arc-free operating conditions. Therefore, the method is used for many applications, including solar control and low-emissivity coatings, barrier layers on packaging, flat panel displays and solar cells. Besides, very long-term process stability, reduced defect density, improved film properties and enhanced dynamic deposition rates are important for good adhesion of the corresponding films. TiO$_2$ films obtained by magnetron sputtering are widely used as high-refractive-index dielectric layers in multi-layer optical devices and functional films [13]. It is well known, however, that the optical properties of titania films, as well as their stability, are critically dependent on the film structure, which in turn is dependent on the deposition conditions used [14-16].

The film obtained by PMS in our experiments shows very low extinction coefficients for wavelengths higher than 500 nm, indicating its potential to be applied as laser, because low energy excitation is enough for the inverse electron population (higher electron density in excited state then in ground state).

2. Experimental methods and materials

2.1. Deposition of Ti_xO_y films

The Ti_xO_y coating was deposited onto glass substrate (20x40x2 mm) using a magnetron sputtering gun perpendicular to the target surface. Before deposition, the substrate was ultrasonically cleaned in propanol and then sputter cleaned. The SiO_2 glass substrates were fixed on a rotating heater, arranged at 45°, and cleaned by DC sputtering at 10 kV (2000 A) for 8.30 min. Prior to sputtering the chamber was evacuated to the pressure of 0.04 Pa and then oxygen was introduced to the pressure of 2000 Pa.

The Ar: O_2 ratio of 0.12 in the gas mixture (total pressure was about 0.5 Pa) was used for the deposition. A 76 mm Ti target (cathode) without pronounced erosion track was employed, and the depositions were performed using an advanced energy power supply coupled to a MELEC 2000A high power pulsing unit, which was set to deliver pulses with an on-time of 50 μs and a frequency of 0.5 kHz. The film was grown at a constant average target current of 1 A without external heating of the substrate, while the target-to-substrate distance was kept at 40 mm. The substrate temperature, measured during the deposition using a Pt-100 thermo-resistor clamped onto substrate, was found to be about 150 °C at all deposition conditions.

After the deposition, the sample was further thermally treated at 400 °C for 1 hour. Ti_xO_y films were grown at the process pressure of 0.5 Pa.

2.2. Characterization of the TiO_x film

The phase composition of the thin film obtained by PMS was analyzed by a Philips PW 1050 powder diffractometer using Ni-filtered Cu-K_λ radiation (λ = 1.5418 Å). The diffraction intensity was measured in the 2θ range from 10° to 70° with a step size of 0.02° and exposition time of 2s per step.

FTIR (Nicolet IS 50 FT-IR Spectrometer) method was used for the additional phase composition analysis of the thin films obtained by PMS.

XPS depth profiling was carried out on a SPECS customized UHV surface analysis system containing sputter ion gun, PHOIBOS 100 spectrometer for energy analysis, dual anode Al/Ag monochromatic source and electron flood gun. XPS spectra were taken using monochromatic Al Kα line (photon energy of 1486.74 eV) in FAT 20 mode with energy step of 0.1 eV and dwell time of 1-2 s depending on the considered line. The main lines of oxygen, titanium, carbon, nitrogen and copper (including its Auger line) were followed during the ion sputtering by 5 keV Ar$^+$ ion beam. The incident angle was 40° with respect to the sample surface. The sputtered area was about 5x5 mm^2, and the typical primary beam current was about 1.8 μA. The working pressure during the measurements was about 1.10^{-8} mbar.

The morphology/topography of the film surface was observed using a scanning electron microscope (SEM JEOL JSM-6460).

Ellipsometric analysis was performed using a J.A. Woollam variable angle spectroscopic ellipsometer (Model VB-400) and the estimation of optical parameters was performed by the ellipsometric analysis program WVASE32. The ellipsometric analysis was performed to: 300-2500 nm and 50, 60, 70 degrees.

3. Results and discussion

3.1. Phase composition of Ti_xO_y films

XRD spectrum of Ti_xO_y film obtained by PMS is shown in Fig.1. Peaks characteristic to anatase (planes (101) and (200) at 25.36 and 48.14°, respectively) [17], rutile (R) (planes (110), (101) and (111) at 27.10, 36.02 and 41.61 °, respectively) [18], TiO (planes (111), (031) and (220) at 29.95, 37.27 and 43.11°, respectively) [19], Ti_2O_3 (planes (012), (110), (024) and (300) at 23.19, 34.87, 48.38 and 62.66°, respectively) [20], and Ti_3O_5 (planes (020), (110) (113) and (220) at 18.27, 25.61, 37.72 and 43.08°, respectively) [21] can be observed. The amorphous hallo in the 20°-30°range stems from the glass substrate, as shown in the Fig, 1 because the film is very thin as shown in the section 3.5.
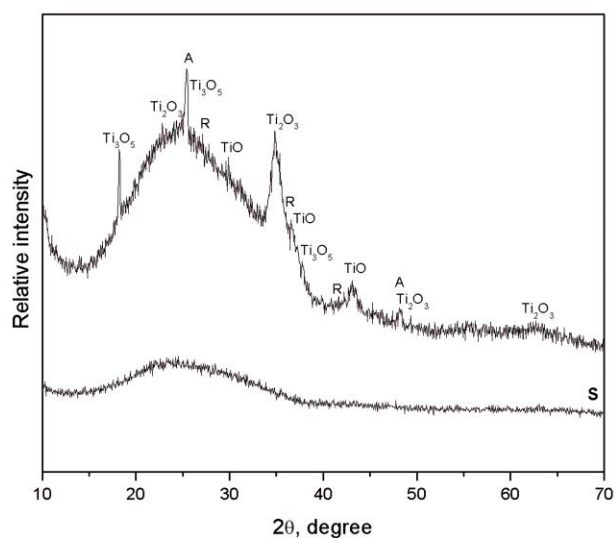

Fig. 1. XRD patterns of Ti_xO_y film obtained by PMS (s- substrate)

3.2. FTIR analysis

FTIR spectrum of Ti_xO_y film obtained by magnetron sputtering is shown in Fig.2. The bands at 2323-1950 cm^{-1} which can be assigned to the overtone of the v(C–O) vibration, belong to CO^{2-} adsorbed on the titanium surface [22, 23]. The band at 852 cm^{-1} corresponds to Ti suboxides (Ti_3O_5). The band at 663 cm^{-1} can be assigned to the TiO_6 octahedron, related to Ti-O stretching bonds, corresponding to rutile phase. The bands between 560-601 cm^{-1} show the presence of Ti-O and Ti-O-Ti stretching vibrations. The peak at 558 cm^{-1} shows the presence of Ti-O and Ti-O-Ti stretching vibrations, while the bands 553-535 cm^{-1} can be assigned also to surface phonon splitting

of the vibration corresponding to band at 663 cm^{-1} influenced by small particle size of anatase either rutile phase. The bands 522-490 cm^{-1} band may correspond to the TP phonon frequency of TiO$_2$ in the rutile phase, but also to the presence of Ti$_3$O$_5$. The bands between 450-440 cm^{-1} can be assigned to vibrations of TiO$_6$ octahedron, related to Ti-O stretching bonds either directed to the interlayer space or to the outer surface formed nanotube, or the TP phonon frequency of rutile phase. The bands at 424 and 407 cm^{-1} can be assigned either to anatase or rutile phase. [24]
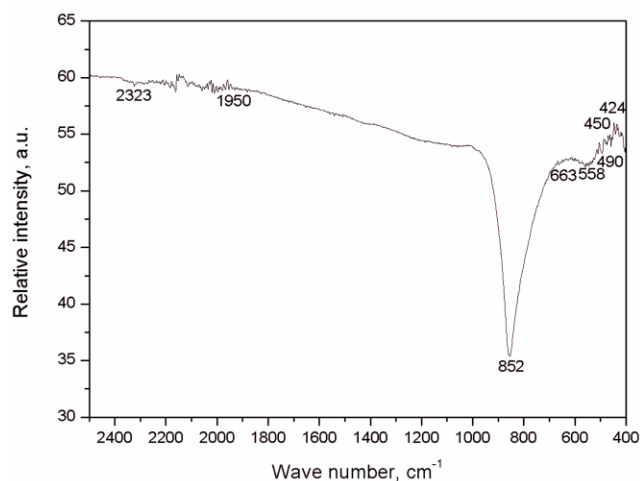

Fig. 2. FTIR spectra of Ti$_x$O$_y$ films obtained by magnetron sputtering

3.3. XPS analysis

XPS spectrum of oxygen O 1s photoelectron line is presented in Fig. 3a, while the O1s fitting results are summarized in Table 1. The dominant contribution situated at about 530.1 eV, denoted as peak 1, can be readily attributed to TiO$_2$ and Ti$_2$O$_3$ phases [24]. Its high relative intensity (typically 90 %) is a clear indication that these oxides are dominant. The relative amount of peak 2 cannot be correlated with the detected amounts of hydrocarbons or the TiO phase (see below), implying it is most probably a consequence of nonuniform surface charging. Peaks 3 and 4 which appear only at the surface are related to the hydrocarbon contamination eg. O-(C=O)-O group [25].

Table 1. O 1s line, fitting results

Measure-ment	Peak 1 (eV/%)	Peak 2 (eV/%)	Peak 3 (eV/%)	Peak 4 (eV/%)
as received	530.1/76.0	531.5/13.0	532.5/8.3	533.8/2.7
1st sputtering	530.1/90.1	531.8/9.9	-	-
2nd sputtering	530.3/91.7	531.8/8.3	-	-
3rd sputtering	530.2/92.0	531.7/8.0	-	-
4th sputtering	530.3/90.6	531.8/9.4	-	-
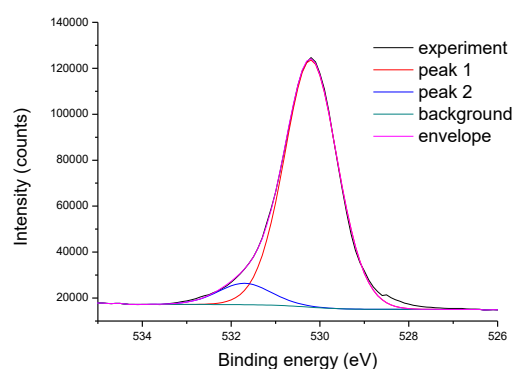
a)
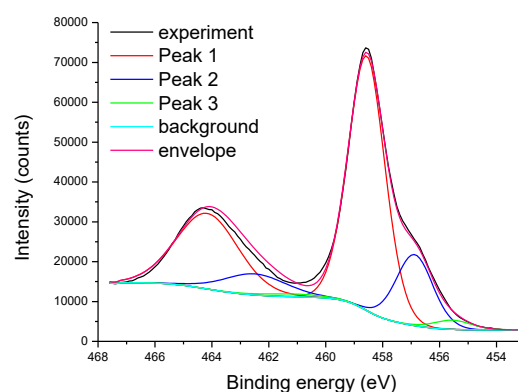
b)

Fig. 3. O 1s (a) and Ti 2p (b) photoelectron lines measured after the 3rd sputtering cycle, and the corresponding fitting result

Typical XPS spectrum of the Ti 2p line, shown in Fig. 3b, can be fitted to three contributions having Ti2p$_{3/2}$ line situated at about 458.6 eV, 457.1 eV and 455.4 eV, respectively. The fitting results are given in Table 2. These contributions can be readily attributed to TiO$_2$ (peak 1), Ti$_2$O$_3$ (peak 2) and TiO (peak 3) (Table 2). The peak which appears after the fourth sputtering does not have a simple interpretation. It could be related to some Ti phase with the oxidation state between Ti(II) and Ti(III), but also a consequence of non-uniform sample charging.

Table 2. Ti 2p line fitting results (only positions of the Ti 2p$_{3/2}$ are presented)

Measure-ment	Peak 1 (eV/%)	Peak 2 (eV/%)	Peak 3 (eV/%)	Peak 4 (eV/%)
as received	458.6/100	-	-	
1st sputtering	458.6/89.1	457.1/9.4	455.5/1.5	
2nd sputtering	458.6/84	457.0/14.6	455.4/1.4	
3rd sputtering	458.6/76	456.9/21.2	455.5/2.7	
4th sputtering	458.6/66.6	457.2/21.1	455.1/1.2	456.4/11.1

We can conclude that the surface (as received) of the thin film contains TiO_2 phase only, while during the sputtering (1st-3rd) phases with lower Ti oxidation states (Ti_2O_3 and TiO) appear. Apparently, in deeper layers the amount of phases with Ti lower oxidation states (Ti(III) and Ti(II)) increase, although this could also be attributed to preferential sputtering effect which contributes to the decrease of the relative oxygen amount [26]. XPS technique is not reliable in detecting Ti_3O_5 phase. It is expected that its contribution should be somewhere in-between those of TiO_2 and Ti_2O_3 [27], so it is very hard to resolve it. Besides, to the best of our knowledge, there is no reliable XPS measurement of the reference Ti_3O_5 spectrum in the literature which would provide its exact position.

3.4. Spectroscopic ellipsometry

Spectroscopic ellipsometry was used to gain a deep insight into various optical properties of Ti_xO_y film, like film thickness, refractive index, extinction coefficients, and others, which can be derived from these properties. After the ellipsometric data are acquired, in the range 300 – 2500 nm, a fitting procedure to calculate the optical parameters and thickness was used to minimize the mean square error (MSE) that is given by:

$$MSE = \sqrt{\frac{1}{2N-M}\sum_{i=1}^{N}\left[\left(\frac{\psi_i^{mod}-\psi_i^{exp}}{\sigma_{\psi,i}^{exp}}\right)^2+\left(\frac{\Delta_i^{mod}-\Delta_i^{exp}}{\sigma_{\Delta,i}^{exp}}\right)^2\right]} \quad (1)$$

where N is the number of (Ψ, Δ) pairs, M is the number of variable parameters in the model, and σ are the standard deviations on the experimental data points.

To interpret the ellipsometric data it has been necessary to create an appropriate model. Typical models used for data fitting consist of substrate/layer1/…/layerN. In this case a single-layer model was carried out: substrate/TiO_2(graded)/roughness.

To describe the properties of titanium oxide layer a graded layer was used, in particular this type of layer is used to simulate a layer which is inhomogeneous in the direction perpendicular to the sample surface. Many films will exhibit non-uniform optical properties along the direction of the film normal. This may be due to drift of the deposition parameters during the film deposition, and may also be due to post-deposition processing of the film. In our case we mixed titanium and titanium oxide materials together using an effective medium approximation. The fitted and experimental data were compared in Fig.4 and the good agreement of data showed that a correlation between refractive index and thickness is well controlled.
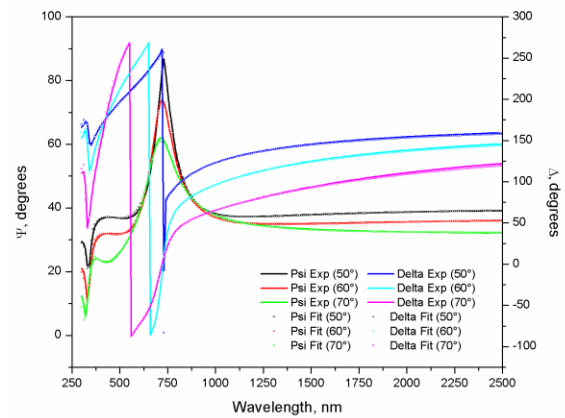

Fig. 4. Generated and experimental data of the sample

The refractive index decreased significantly with wavelength in the range 300 - 500 nm and for longer wavelengths it decreased slightly (Fig. 5).

The extinction coefficient decreased with increasing wavelength, reaching value less than 0.01 at wavelengths higher than 500 nm. This property may be of significance for potential application of the system as lasers for wavelengths higher than 500 nm.
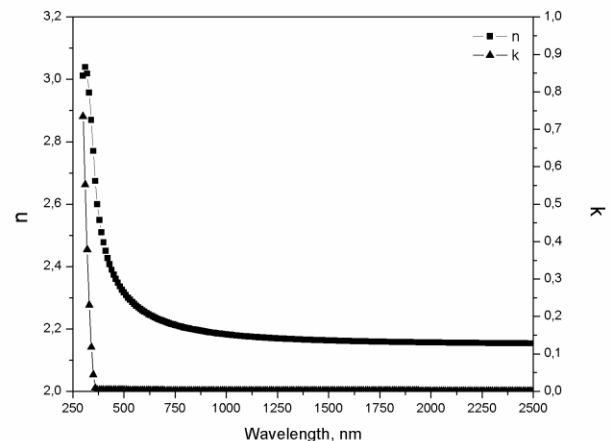

Fig. 5. Refractive index (n) and extinction coefficient (k) vs. wavelength of titanium oxide graded layer

3.5. Morphology

As it can be seen in Fig. 6, the film surface has pretty developed morphology with rod-shaped and snowflake-shaped particles. Snowflake particles are of different sizes, with different degree of branching. The length of principal branches is from about 0.4 to 1.9 μm while side branches are from 0.25 to 0.65 μm long. These particles might be TiO_2 crystals. Rod-shaped particles are about 4 μm long and they correspond to rutile or anatase phase.
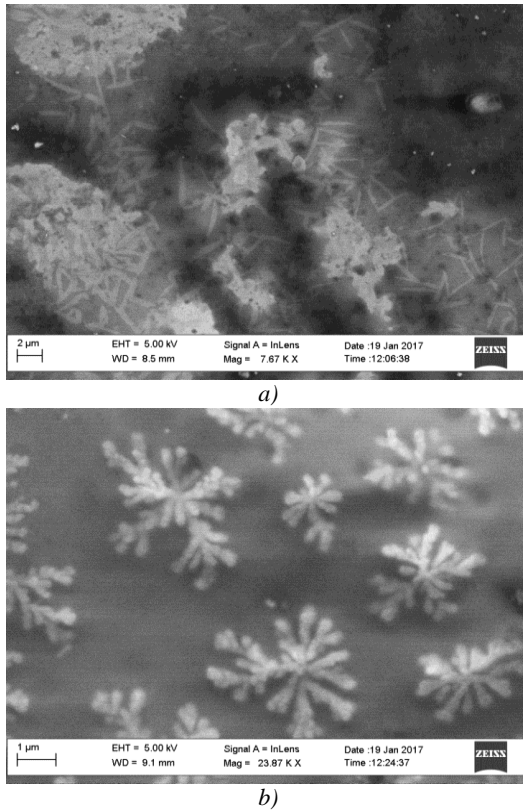
Fig. 6. Typical appearance of Ti$_x$O$_y$ film obtained by PMS: a) magnification 7670x, b) magnification 23870x

From microanalysis it can be noted that the sample is homogeneous on surface, thickness of approximately 125 nm, which is in agreement with spectroscopic ellipsometry findings (Fig. 7).

Fig. 7. Film thickness

EDS analysis revealed the presence of Ti and O, but also the presence of C due to hydrocarbon contamination on the film surface, and Si belonging to glass substrate (Fig. 8).
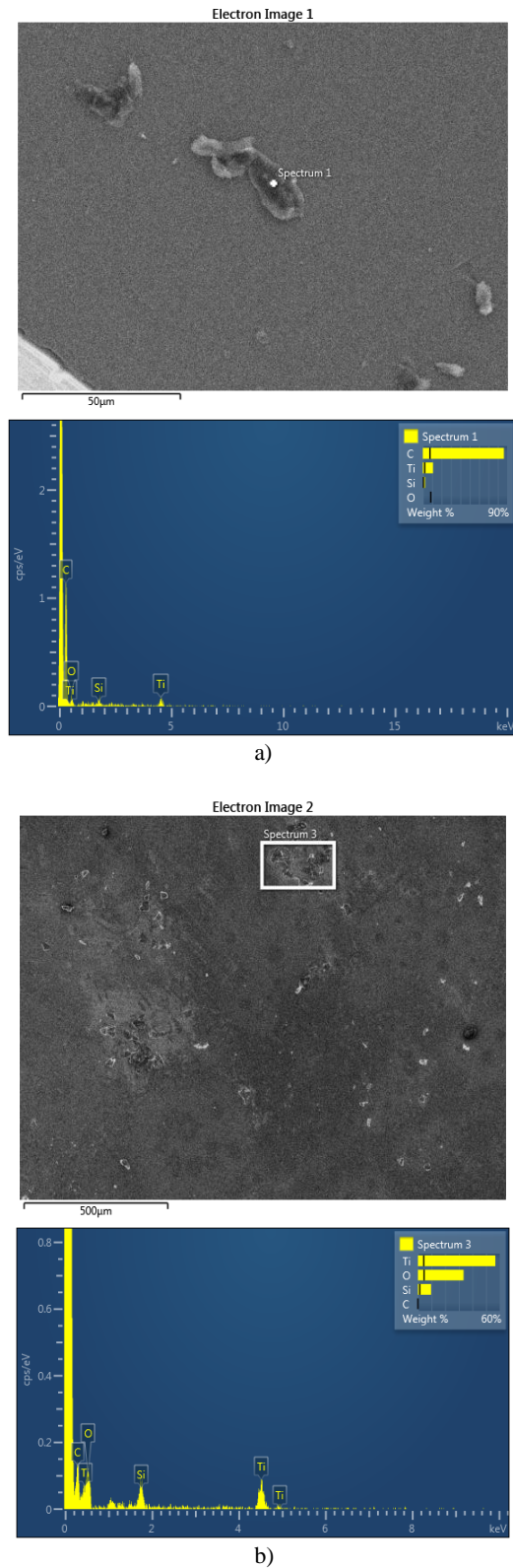

Fig. 8. a) and b) EDS spectra of various parts of Ti$_x$O$_y$ film obtained by PMS

4. Conclusions

Ti$_x$O$_y$ thin film, with thickness of 125 nm, was obtained by pulsed magnetron sputtering. The film was mainly constituted of an amorphous and crystal phases of anatase, rutile, TiO, Ti$_2$O$_3$ and Ti$_3$O$_5$. The film exhibited parabolic decrease of the refractive indices with wavelength and low values of the extinction coefficients (less than 0.01) at 500 nm and higher wavelengths due to which these films may be suitable for high-power laser applications.

Acknowledgments

References

[1] P. J. Kelly, P. S. Henderson, R. D. Arnell, G. A. Roche, D. Carter, J. Vac. Sci. Technol. **A18**, 2890 (2000).

[2] J. O'Brien, P. J. Kelly, Surf. Coat. Technol. **621**, 142 (2001).

[3] P. S. Henderson, P. J. Kelly, R. D. Arnell, H. Backer, J. W. Bradley, Surf. Coat. Techn. **174/175**, 779 (2003).

[4] I. Petrov, P. B. Barna, L. Hultman, J. E. Greene, J. Vac. Sci. Technol., **A21**, S117 (2003).

[5] J. Alami, K. Sarakinos, F. Uslu, C. Klever, J. Dukwen, M. Wuttig, J. Phys. D: Appl. Phys. **42**, 115204 (2009).

[6] D. Severin, O. Kappertz, T. Nyberg, S. Berg, M. Wuttig, Thin Solid Films **515**, 3554 (2007).

[7] D. Gloβ, P. Frach, O. Zywitzki, T. Modes, S. Klinkenberg, C. Gottfried, Surf. Coat. Techn. **200**, 967 (2005).

[8] J. Alami, K. Sarakinos, F. Uslu, M. Wuttig, J. Phys. D: Appl. Phys. **42**, 015304 (2009).

[9] J. Alami, P. Eklund, J. Emmerlich, O. Wilhelmsson, U. Jansson, H. Hogberg, L. Hultman, U. Helmersson, Thin Solid Films **515**, 1731 (2006).

[10] Y. Totik, J. Coat. Technol. Res. **7**(4), 485 (2010)

[11] M. Kadoshima, M. Hiratani, Y. Shimamoto, K. Torii, H. Miki, S. Kimura, T. Nabatame, Thin Solid films **424**, 224 (2003).

[12] N. Martin, R. Sanjines, J. Takadoum, F. Levy, Surf. Coat. Techn. **142**, 615 (2001).

[13] W.H. Kim, H. Kim, H.B.R Lee, J. Coat. Technol. Res. **14**(1), 177 (2017).

[14] O. Treichel, V. Kirchhoff, Surf. Coat. Technol. **123**, 268 (2000).

[15] P. J. Kelly, C. F. Beevers, P. S. Henderson, R. D. Arnell, J. W. Bradley, H. Backer, Surf. Coat. Techn. **174/175**, 795 (2003).

[16] R. D. Arnell, P. J. Kelly, J.W. Bradley, Surf. Coat. Techn. **188/189**, 158 (2004).

[17] C. Legrand, J. Delville, C. R. Hebd. Seances Acad. Sci. **236,** 944 (1953).

[18] E. Sanchez, T. Lopez, R. Gomez, A. Bokimi Morales, A. O. Navaro, J. Solid State Chem. **122** 309 (1996)

[19] D. Watanabe, J.R. Castles, A. Jostons, A. S. Malin, Acta Crystallogr. **23,** 307 (1967).

[20] C. E. Rice, W. R. Robinson, Mater. Res. Bull. **11**(11), 1355 (1976).

[21] A. A. Rusakov, G. S. Zhdanov, Dokl. Akad. Nauk SSSR **77**, 411 (1951).

[22] V. Jokanović, B. Čolović, N. Jović, B. Babić-Stojić, Int. J. Appl. Ceram. Technol., **10**, 957 (2013)

[23] V. Jokanović, M. Vilotijević, B. Jokanović, M. Jenko, I. Anžel, D. Stamenković, V. Lazić, R. Rudolf, Corr. Sci. **82** 180 (2014).

[24] M. C. Biesinger, L. W. M. Lau, A. Gerson, R. S. C. Smart, Appl. Surf. Sci. **257,** 887 (2010).

[25] G. Beamson, D. Briggs, "High Resolution XPS of Organic Polymers - The Scienta ESCA300 Database", Wiley, Chichester, 1992.

[26] A. R. Gonzáles-Elipe, G. Munuera, J. P. Espinos, J. M. Sanz, Surf. Sci. **220,** 368 (1989).

[27] C. Oviedo, J. Phys: Condens. Matter. **5,** A153 (1993).

*Corresponding author: vukoman@vinca.rs